Received: 16 September 2021 | Revised: 7 February 2022 | Accepted: 7 February 2022

DOI: 10.1111/jnc.15588

Journal of Neurochemistry JNC The Official Journal of the International Society for Neurochemistry WILEY

ORIGINAL ARTICLE

LRRK2-G2019S mice display alterations in glutamatergic synaptic transmission in midbrain dopamine neurons

Olga Skiteva | **Ning Yao** | **Giacomo Sitzia** | **Karima Chergui**

Molecular Neurophysiology Laboratory, Department of Physiology and Pharmacology, Karolinska Institutet, Stockholm, Sweden

Correspondence
Karima Chergui, Molecular Neurophysiology Laboratory, Department of Physiology and Pharmacology, Karolinska Institutet, BioClinicum J5:20 Neuro, Visionsgatan 4, 171 64 Solna, Sweden.
Email: karima.chergui@ki.se

Present address
Giacomo Sitzia, Giacomo Sitzia, Laboratory for Integrative Neuroscience, National Institute on Alcohol Abuse and Alcoholism, US National Institutes of Health, Rockville, Maryland, USA

Funding information
Åhlén-stiftelsen; Gun & Bertil Stohnes Stiftelse; Karolinska Institutet; Loo och Hans Ostermans Stiftelse för Medicinsk Forskning; Parkinson Research Foundation (Sweden); Parkinsonfonden; Stiftelsen för ålderssjukdomar vid Karolinska Institutet; Vetenskapsrådet, Grant/Award Number: 2018-02979

Abstract

The progressive degeneration of dopamine (DA) neurons in the substantia nigra compacta (SNc) leads to the emergence of motor symptoms in patients with Parkinson's disease (PD). To propose neuroprotective therapies able to slow or halt the progression of the disease, it is necessary to identify cellular alterations that occur before DA neurons degenerate and before the onset of the motor symptoms that characterize PD. Using electrophysiological, histochemical, and biochemical approaches, we have examined if glutamatergic synaptic transmission in DA neurons in the SNc and in the adjacent ventral tegmental area (VTA) was altered in middle-aged (10–12 months old) mice with the hG2019S point mutation (G2019S) in the leucine-rich repeat kinase 2 (*LRRK2*) gene. G2019S mice showed increased locomotion and exploratory behavior compared with wildtype (WT) littermates, and intact DA neuron integrity. The intrinsic membrane properties and action potential characteristics of DA neurons recorded in brain slices were similar in WT and G2019S mice. Initial glutamate release probability onto SNc-DA neurons, but not VTA-DA neurons, was reduced in G2019S mice. We also found reduced protein amounts of the presynaptic marker of glutamatergic terminals, VGLUT1, and of the GluA1 and GluN1 subunits of AMPA and NMDA receptors, respectively, in the ventral midbrain of G2019S mice. These results identify alterations in glutamatergic synaptic transmission in DA neurons of the SNc and VTA before the onset of motor impairments in the LRRK2-G2019S mouse model of PD.

KEYWORDS
dopamine neurons, glutamate, LRRK2-G2019S, Parkinson's disease, substantia nigra compacta, ventral tegmental area

Abbreviations: aCSF, artificial cerebrospinal fluid; BAC, bacterial artificial chromosome; DA, dopamine; DAT, dopamine transporter; EPM, elevated plus maze; EPSC, excitatory postsynaptic current; LRRK2, leucine-rich repeat kinase 2; PD, Parkinson's disease; RRID, Research Resource Identifier (see scicrunch.org); SNc, substantia nigra pars compacta; TH, tyrosine hydroxylase; VGLUT1, vesicular glutamate transporter 1; VTA, ventral tegmental area.

Olga Skiteva and Ning Yao contributed equally to the paper.

1 | INTRODUCTION

In Parkinson's disease (PD), the progressive degeneration of dopamine (DA) neurons in the substantia nigra pars compacta (SNc), causes motor features that include slowness of movements, muscle rigidity, gait abnormalities, and tremor at rest (Sveinbjornsdottir, 2016). Identification of the neuronal alterations that occur before the onset of motor symptoms, that is, before the loss of SNc-DA neurons, is central to the understanding of PD pathophysiology and can contribute to the design of early interventions that would slow or halt the progression of the disease. Most PD cases are sporadic, with aging as the main risk factor for developing the disease, but familial forms because of mutations in several identified genes occur in approximately 10% of PD patients (Spatola & Wider, 2014). Mutations in the leucine-rich repeat kinase 2 (*LRRK2*) gene (*PARK8*, encoding dardarin protein), are among the most common causes of familial PD, producing autosomal dominant late-onset PD that is similar to idiopathic PD. The G2019S point mutation is a common, and the most studied, pathogenic mutation in the *LRRK2* gene (Healy et al., 2008; Hernandez et al., 2016; Spatola & Wider, 2014). This mutation affects the serine/threonine kinase domain of the LRRK2 protein which leads to increased kinase activity (Yue et al., 2015). Increased LRRK2 kinase activity and G2019S mutation are also observed in sporadic PD (Di Maio et al., 2018; Healy et al., 2008), demonstrating the importance of LRRK2 in the pathogenesis of the disease.

It has recently been recognized that presynaptic alterations play important roles in neurodegenerative diseases and that these changes occur in the early, prodromal phase of PD, preceding DA neuron loss (Gcwensa et al., 2021). Given that excessive glutamate release can lead to neurotoxicity and neuronal death (Wang et al., 2020), it is possible that an altered LRRK2 function in glutamatergic synapses onto SNc-DA neurons contributes to G2019S-linked PD pathology. LRRK2 is present in brain regions that provide glutamatergic inputs to midbrain DA neurons, that is, cortex, hippocampus, and subthalamic nucleus (Giesert et al., 2013; Higashi et al., 2007; Kuhlmann & Milnerwood, 2020; Melrose et al., 2006; Vitte et al., 2010; West et al., 2014). However, changes in glutamatergic synaptic transmission in SNc-DA neurons have not been investigated in LRRK2 mutant rodents. Alterations in glutamatergic synaptic transmission and plasticity have been identified in the striatum, cortex, and hippocampus of rodents bearing the LRRK2-G2019S mutation, demonstrating a role for LRRK2, and altered function of mutated LRRK2, in excitatory neurotransmission in these brain regions (Beccano-Kelly et al., 2014; Chen et al., 2020; Chou et al., 2014; Li et al., 2010; Matikainen-Ankney et al., 2016; Sweet et al., 2015; Tozzi et al., 2018; Volta et al., 2017). It is possible that the G2019S mutation in the *LRRK2* gene modifies glutamatergic synaptic transmission in SNc-DA neurons. Indeed, LRRK2 protein was detected in low amounts in DA neurons (Higashi et al., 2007; Kuhlmann & Milnerwood, 2020; Vitte et al., 2010), and conditional expression of LRRK2-G2019S in catecholaminergic neurons leads to age-dependent degeneration of DA and noradrenergic neurons, suggesting that increased LRRK2 kinase function in these neurons contributes to their death (Cresto et al., 2020; Xiong et al., 2018).

LRRK2 dysfunctions in midbrain DA neurons might play a role in anxiety and depression, non-motor symptoms that are common in PD patients during the disease and before the motor symptoms develop (Lim & Lang, 2010; Richard, 2005). In addition to their role in motor functions, midbrain DA neurons have a critical role in reward processing and motivation (Russo & Nestler, 2013). An altered glutamatergic neurotransmission in midbrain DA neurons, in particular those located in the ventral tegmental area (VTA), a nucleus adjacent to the SN, could be implicated in anxiety and depression (Russo & Nestler, 2013). Remarkably, VTA-DA neurons are less vulnerable to degeneration than SNc-DA neurons in PD, possibly because of cellular and molecular differences between these two brain regions (Brichta & Greengard, 2014). Our aims were to determine whether abnormalities in glutamatergic synaptic transmission occur in midbrain DA neurons, whether these abnormalities are rescued by the LRRK2 kinase inhibitor LRRK2-IN-1, and whether there are regional differences, in middle-aged (10–12 months) G2019S transgenic mice, when degeneration of DA neurons has not started (Li et al., 2010).

2 | MATERIALS AND METHODS

2.1 | Animals

The study was not pre-registered and was designed to be exploratory. No randomization was performed to allocate subjects in the study and no blinding was performed. Sample size was not calculated a priori but was estimated based on previous studies (Feng et al., 2014; Lim et al., 2018; Sitzia et al., 2020), and verified by post hoc power analysis. Animal experiments were approved by our local ethical committee (Stockholms norra djurförsöksetiska nämnd, 20464–2020). We used bacterial artificial chromosome (BAC) LRRK2-G2019S mice which express a mutant form of human LRRK2. These mice were obtained from The Jackson laboratory (C57BL/6J-Tg[LRRK2-G2019S]2AMjff/J, JAX stock #018785; RRID:IMSR_JAX:018785) and were mated as Noncarrier x Hemizygote. Several studies have previously characterized and validated these mice and demonstrated that the observed neuronal alterations resulted from an increased G2019S-linked LRRK2 kinase inhibition (Belluzzi et al., 2016; Marte et al., 2019; Melrose et al., 2010; Pischedda et al., 2021; Qin et al., 2017; Volta et al., 2015). Mice were housed in small groups (2–5 per cage, IVC Mouse—GM500) in a humidity-controlled room with a 12:12 h light/dark cycle and had free access to food and water. We used male and female, 10–12 months old, hemizygous mice (G2019S) and non-transgenic wildtype (WT) littermates. No animal died during the course of the experiments except when sacrificed. The experiments using mice, except for the behavioral experiments, were of terminal type, under deep anesthesia. Male and female mice were compared for all the experiments in our study and significant sex-related differences, if present, were described in

the results. A total of 174 mice were used in the present study. Since we breed our mice, we use them when they become available, and when they have reached 10–12 months of age. We have therefore included, in our studies, all the mice that were available, and we did not assign a specific number of mice to the different experimental groups. Therefore, there is some variability in the numbers of mice used in the different experiments, in particular the numbers of male and female mice. The number of mice used for immunohistochemistry is lower than the number of mice used for Western blotting because there is generally less variability with immunohistochemistry than with western blotting and because we frequently use the same mouse to prepare brain slices that are used for either the electrophysiological experiments or for Western blotting. A total of 10 mice were used for immunohistochemistry: eight mice (four WT and four G2019S) were used for counting TH-positive cells in the SNc and VTA (Figure 2b,c), and two mice (one WT and one G2019S) were used for co-labeling of TH with GluA1 or GluN1 (Figure 5a,b). The experimental design is illustrated in Figure 1a.

2.2 | Behavioral tests

The behavioral experiments were performed between 12.00 and 16.00. Mice in their home cages were transferred to the testing room, located in the same housing facility, and allowed to adapt for at least 30 min before the test was initiated. The behavioral tests were performed under this sequence for most mice: open field, light dark, elevated plus maze, pole test, and beam test.

2.3 | Open field test

Mice were placed individually in the center of an open field arena (48 cm × 48 cm; TSE systems, available at the Animal Behavior Core Facility at Karolinska Institutet) and allowed to move in the arena for 60 min during which horizontal and vertical spontaneous locomotor activity was tracked. Data were analyzed by TSE software automatically (TSE ActiMot detection system, Version 08.02.03, TSE Systems GmbH, Bad Homburg, Germany). We analyzed the total distance covered, the number of rearings, and the time spent in the center and in the periphery of the arena. The periphery was defined as the peripheral 40% of the arena and the center as 60% of the arena.

2.4 | Light/dark box test

We used a light/dark box arena which had an area with light (light area: 25 cm × 25 cm, 350 lux), and an area that was dark (dark area: 25 cm × 12 cm, 0.5 lux). Male mice were placed individually in the light area of the arena, facing the port entry of the dark area, and were allowed to explore the arena for 15 min. The movements of the mouse were video tracked using a video camera mounted in the ceiling and coupled to the EthoVision XT11.5 software (RRID:SCR_000441, Noldus). The time spent in the light area and the number of entries in the light area during the 15 min of the trial were analyzed.

2.5 | Elevated plus maze (EPM) test

We used an EPM which consisted of two open arms (35 × 10 cm each) and two closed arms (35 × 10 cm each), elevated by 50 cm above the floor. Male mice were placed individually in the center of the EPM, facing an open arm, and were able to explore the platform for 5 min during which they were video tracked as in the light/dark box test with the EthoVision XT11.5 software (RRID:SCR_000441, Noldus). The time spent in the open arms and the number of entries in the open arms were analyzed. Male mice were used in this test and in the light/dark box test because variations of estrous cycle often influence the performance of female mice (Gould, 2009).

2.6 | Beam walking test

Mice were placed individually on one end of an elevated horizontal beam (3.5–1 cm wide and 1 m long). They were trained during the first 2 days of the test to traverse the beam and reach the other end of the beam where their home cage was placed. On the third day of the test, a metal mesh of the same width and length as the beam was placed 1 cm above the beam, mice were videotaped while traversing the beam for a total of three trials. We measured, manually with a timer, and averaged the time taken by the mice to traverse the beam and the number of paw slips during the traversal of the beam for the three trials.

2.7 | Pole test

Mice were placed individually on top of a vertical pole (diameter: 8 mm, height: 50 cm) with their head facing upwards. They were trained during the first 2 days of the test to turn and descend the pole back into a cage. On the third day of the test, we measured, manually with a timer, the time taken by the mice to turn downward (Tturn) and the total time to descend the pole (Ttotal). Mice were videotaped while descending the pole for a total of three trials, and we calculated the average of the three trials.

2.8 | Brain slice electrophysiology

Mice were deeply anesthetized with isoflurane. Isoflurane was chosen because it offers several benefits over other anesthetic agents. Anesthetized mice underwent transcardiac perfusion

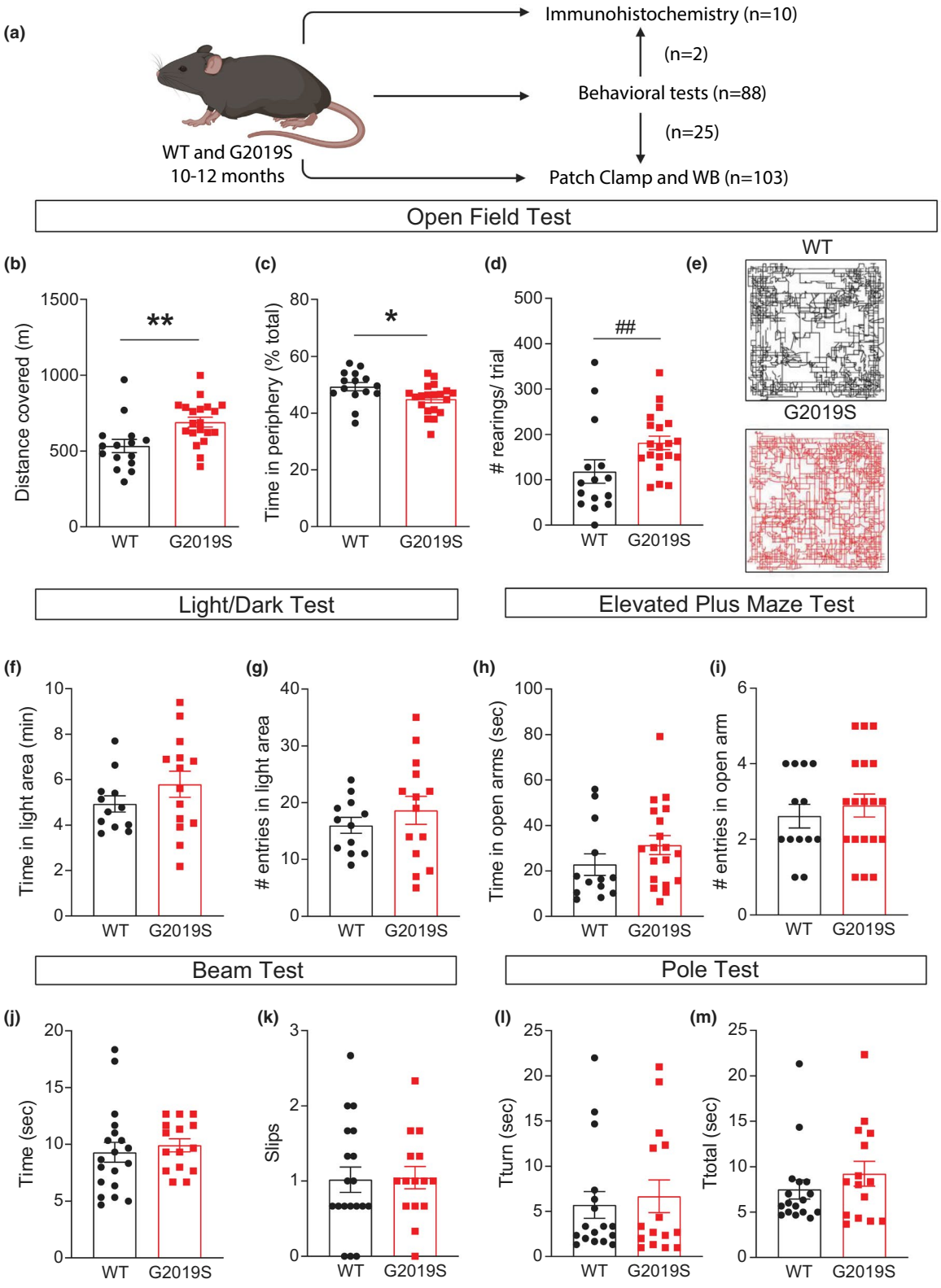

FIGURE 1 Assessment of motor and non-motor behaviors in WT and G2019S mice. Flow-chart illustrating the experimental design (a). Spontaneous horizontal locomotion and rearing were measured in the open field test (b–e). Panel (e) shows typical tracks for a WT mouse and a G2019S mouse during the first 10 min of the trial. $^{*}p < 0.05$; $^{**}p < 0.01$ Student's unpaired *t*-test; ## $p < 0.01$ Mann–Whitney test. Anxiety-like behavior was assessed with the light/dark test (f, g) and the EPM test (h, i). Fine motor coordination and balance were assessed with the beam walking test (j, k) and the pole test (l, m). Results are mean ± s.e.m. from $n = 12$–20 mice: open field test, WT $n = 15$, G2019S $n = 20$; light/dark test, WT $n = 12$, G2019S $n = 14$; EPM, WT $n = 13$, G2019S $n = 19$; Pole test, WT $n = 17$, G2019S $n = 15$; Beam test, WT $n = 19$, G2019S $n = 15$

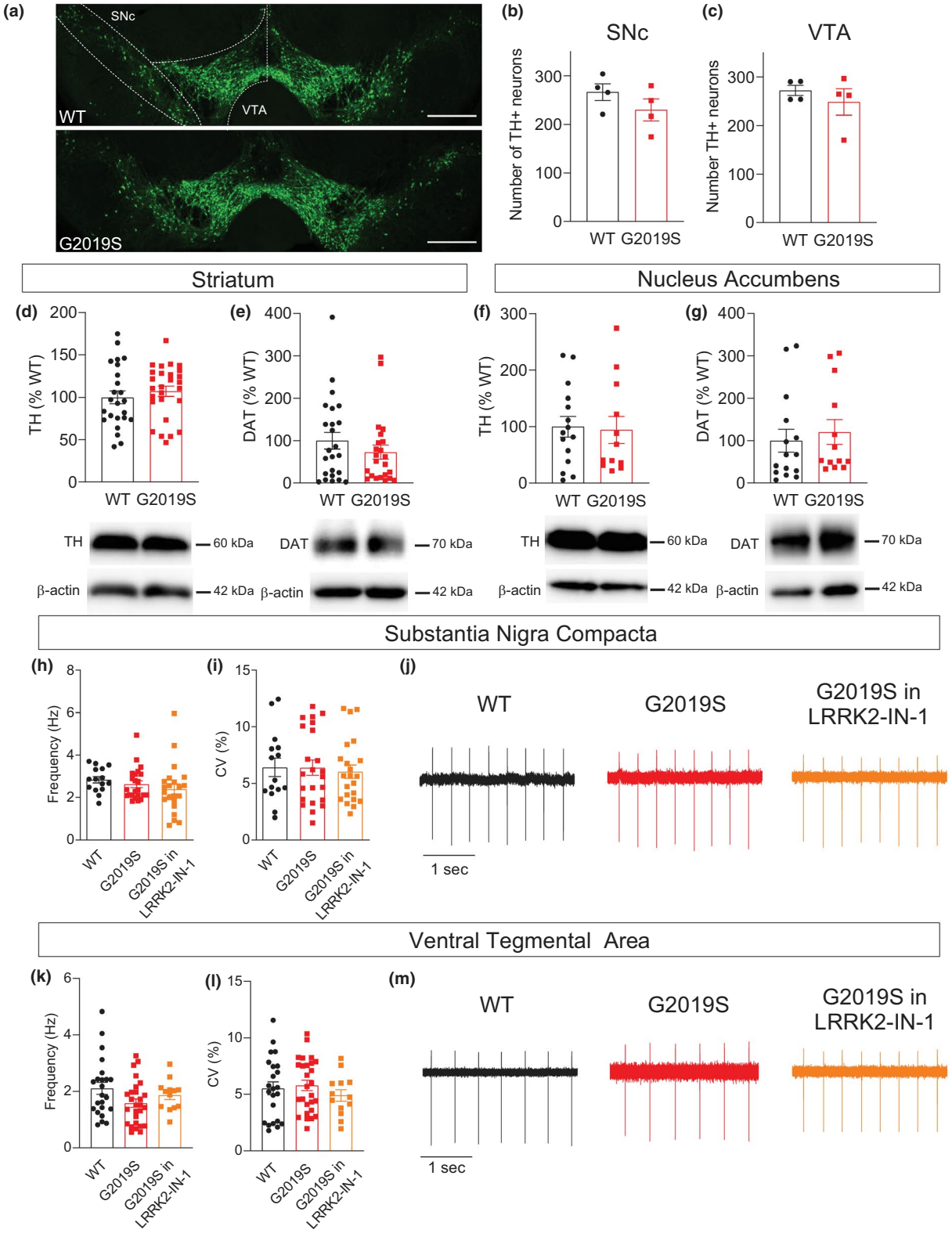

FIGURE 2 Integrity of SNc- and VTA-DA neurons. (a) Confocal images showing immunofluorescence for TH in the VTA and SNc of a WT mouse and a G2019S mouse (Scale bars 500 μm, 18 z-stacks with 2 μm interval). (b, c) Number of TH-positive cells in the SNc and VTA of WT mice ($n = 4$ mice) and G2019S mice ($n = 4$ mice). (d–g) Western blotting of TH and DAT in the striatum ($n = 24$ WT mice and $n = 23$–27 G2019S mice) and nucleus accumbens ($n = 15$ WT mice and $n = 12$–13 G2019S mice). (h–m) Frequency (Hz) and coefficient of variation (CV, %) of the spontaneous firing, measured in cell-attached mode, of SNc- (h, i) and VTA-DA neurons (k, l) ($n = 15$–23 cells from four to seven WT mice and $n = 23$–27 cells from seven G2019S mice). Traces in (j) and (m) are example recordings from SNc- and VTA-DA neurons in WT and G2019S mice

with 60 ml ice-cold oxygenated (95% O_2 + 5% CO_2) artificial cerebrospinal fluid (aCSF) containing (in mM): NaCl (126), KCl (2.5), NaH_2PO_4 (1.2), $MgCl_2$ (1.3), $CaCl_2$ (2.4), glucose (10), and $NaHCO_3$ (26). Their brains were rapidly removed and submerged in a slicing solution containing (in mM): NaCl (15.9), KCl (2), NaH_2PO_4 (1), Sucrose (219.7), $MgCl_2$ (5.2), $CaCl_2$ (1.1), glucose (10), and $NaHCO_3$ (26). Coronal hemisections (200–250 μm thick) containing the midbrain, the striatum, and the nucleus accumbens were obtained using a microslicer (VT 1000S, Leica Microsystem). The sections were incubated in a modified aCSF containing (in mM): NaCl (126), KCl (2.5), NaH_2PO_4 (1.2), $MgCl_2$ (4.7), $CaCl_2$ (1), glucose (10), and $NaHCO_3$ (23.4) at 32 °C for 1 h following the slicing and afterward at 28°C. We performed cell-attached and whole-cell patch-clamp recordings of visually identified SNc- and VTA-DA neurons, as described previously (Yao et al., 2018). Neurons were identified as being DA based on several anatomical, morphological, and electrophysiological criteria which included the location of these neurons in the VTA and SNc, their slow spontaneous firing (<6 Hz), the presence of an Ih current and membrane capacitance (>40 pF) which characterize DA neurons. Cells that did not meet these criteria were not further recorded and were not included in the analyses. These criteria allowed us to differentiate between DA neurons and non-DA neurons, and our previous study confirmed that the recorded neurons contained tyrosine hydroxylase (TH) (Yao et al., 2018). Patch electrodes (3–5 MΩ) were filled with a solution containing (in mM): 140 CsCl, 2 $MgCl_2$, 1 $CaCl_2$, 10 HEPES, 10 EGTA, 2 MgATP, 0.3 Na_3GTP, pH adjusted to 7.3 with CsOH. For current-clamp recordings, electrodes were filled with a solution containing (in mM): D-gluconic acid potassium salt (120), KCl (20), HEPES (10), EGTA (10), $MgCl_2$ (2), $CaCl_2$ (1), ATP-Mg (2), $GTPNa_3$ (0.3), pH adjusted to 7.3 with KOH. Recordings were performed with a MultiClamp 700B (Axon Instruments, Foster City CA, USA), acquired at 10 kHz and filtered at 2 kHz. Spontaneous firing of DA neurons was measured with tight seal (>500 MΩ) cell-attached recordings at 0 mV. Excitatory postsynaptic currents (EPSCs) mediated by AMPA receptors (AMPARs) were measured at a holding membrane potential of −80 mV, in the whole-cell mode, in the presence of gabazine (SR-95531, 10 μM) to block $GABA_A$ receptors. NMDAR-mediated EPSCs were measured at a holding membrane potential of +40 mV in the presence of DNQX (10 μM), to block AMPARs, and gabazine (10 μM). EPSCs were evoked by electrical stimulations through a patch pipette filled with aCSF placed near the recorded neuron. Paired AMPAR-EPSCs were evoked with interstimulus intervals of 20, 60, 100, 1000, and 3000 ms. Data were acquired and analyzed with the pClamp 10 software (RRID:SCR_011323, Axon Instruments, Foster City CA, USA). Spontaneous EPSCs were recorded for 3–5 min. We analyzed the 3–5 min-long recordings using the Mini Analysis program Synaptosoft (Synaptosoft, Inc.; RRID: SCR_002184) to measure the frequency and amplitude of sEPSCs in individual neurons. For the selection and analysis of sEPSCs, we used an amplitude threshold of 5 pA based on the distribution of noise and sEPSC amplitude.

2.9 | Western blotting

Brain slices were prepared as described for slice electrophysiology. The dorsal striatum, nucleus accumbens, and the ventral midbrain (containing VTA and medial substantia nigra) were dissected from the slices, frozen, and stored at −80°C until processed. The samples were sonicated in 1% sodium dodecyl sulfate (SDS) and boiled for 10 min. One percent SDS was diluted in water from 10% SDS (prepared with 18 MΩ water, Bio-rad, Cat. No. 1610416). Protein concentration was determined in each sample with a bicinchoninic acid protein assay (BCA-kit, Pierce). Equal amounts of protein (10 or 30 μg) were re-suspended in sample buffer (4 × Laemmli Sample Buffer, Bio-Rad, Hercules, USA, added with 10% β-mercaptoethanol, Sigma) and separated by SDS–polyacrylamide gel electrophoresis using a 9% or 12% running gel and transferred to a nitrocellulose transfer membrane (Bio-Rad, Hercules, USA). The membranes were incubated for 1 h at room temperature with 5% (w/v) fat-free dry milk (Bio-Rad, Hercules, USA) in TBS-T (Tris base 0.05 mol/L, NaCl 0.15 mol/L, tween 0.1%). Immunoblotting was carried out with antibodies in 5% dry milk dissolved in TBS-T at 4°C overnight. Antibodies were obtained from Sigma-Aldrich, St Louis, USA (TH, Cat. No. T2928, RRID: AB_2313844, dilution 1:2000; β-actin, Cat. No. A2228, RRID: AB_476697; dilution 1:2000), Millipore, Temecula, US (dopamine transporter [DAT], Cat. No. MAB369, RRID: AB_2190413; dilution 1:1000; VGLUT1, Cat. No. AB5905, RRID: AB_2301751; dilution 1:1000; GluN1, Cat. No. MAB363, RRID: AB_94946; dilution 1:1000), and Upstate, New York, USA (GluA1, Cat. No. 06-306-MN, dilution 1:1000). The membranes were washed three times with TBS-T and incubated, for 1 h at room temperature, with secondary horseradish peroxidase-linked Anti-Rabbit IgG (H + L) (Cat. No. 32260, 1:5000 dilution) or Anti-Mouse IgG (H + L) (Cat. No. 32230, 1:5000 dilution) obtained from Thermo Scientific, Rockford, USA. At the end of the incubation, membranes were washed six times with TBS-T and immunoreactive bands were detected by enhanced chemiluminescence (Bio-Rad, Hercules, USA, Cat. No. 170–5061). The membranes were then scanned in ChemiDoc MP system (Bio-Rad, Hercules, USA) and quantified with ImageJ 1.50b software (NIH, USA). The protein amounts were normalized to the value of β-actin and normalized to the averaged value obtained for WT mice.

2.10 | Immunofluorescence

Mice underwent transcardiac perfusion with saline followed by 4% PFA in PBS (PBS: 0.01 M phosphate buffer, 0.0027 M KCl, 0.137 M NaCl; Carl Roth, Karlsruhe, Germany, Cat. No. P087.7) under deep isoflurane anesthesia. Their brain was removed, post-fixed in 4% PFA overnight, and dehydrated in 30% sucrose-PBS buffer for 2–3 days. Dehydrated brains were embedded in OCT cryomount (Cat. No. 45830, Histolab), frozen at −20°C and sliced with a MICROM cryostat (HM 500 M) at a 40 μm thickness. The sections were collected and stored in NaN_3 (0.01% in PBS) in 24-well plates at 4°C. Free-floating

brain sections containing the midbrain were processed for immunodetection of TH alone or with either GluA1 or GluN1. Sections were incubated for one night at 4 °C in the following primary antibodies: TH (Sigma-Aldrich, St Louis, USA, Cat. No. T2928, dilution 1:4000), TH (Millipore, Temecula, USA, Cat. No. AB152, dilution 1:2000, RRID: AB_390204), GluA1 (Upstate, New York, USA, Cat. No. 06-306-MN, dilution 1:1000), GluN1 (Millipore, Temecula, US, Cat. No. MAB363, dilution 1:1000). Sections were washed 3 times in PBS and incubated in Alexa Fluor® 568-conjugated goat anti-rabbit-IgG (Thermo Scientific, Cat. No. A-11011, dilution 1:2000) or Alexa Fluor® 488-conjugated goat anti-mouse-IgG (Thermo Scientific, Cat. No. A-11001, dilution 1:2000) for 2 h at room temperature, followed by re-washing in PBS and mounting. The sections were imaged on a Carl Zeiss LSM 880 confocal microscope using a 10x objective (NA value: 0.45), a 20x objective (NA value: 0.75) or a 63x oil objective (NA value: 0.8). Images were z-stacked. For counting the number of TH-positive cells, TH immunostaining was performed in four to five sections containing different levels of the SNc and VTA (Bregma −4.80 to 6.04) for each mouse examined. After confocal scanning with a 20x objective, the number of TH-positive cells in SNc and VTA in both sides of each section was counted manually using Cell Counter plugin in Fiji (Schindelin et al., 2012) and a surface cell count method described earlier (Henderson et al., 2020; Moore et al., 2021). The number of cells from the two sides of the same section was added, and the average of all sections was calculated for each mouse.

2.11 | Chemicals and drugs

Salts and other chemicals were purchased from Sigma-Aldrich (St. Louis, USA), Tocris/Bio-Techne Ltd., and Hello Bio (Bristol, UK). The compounds used for slice electrophysiology (DNQX, Cat. No. HB0261; gabazine, SR95531, Cat. No. HB0901; LRRK2-IN-1, Cat. No. 4273/10) were prepared in stock solutions, diluted in aCSF to their final concentration (1 or 10 μM), and applied in the perfusion solution. In the experiments examining the effect of LRRK2-IN-1 on firing and glutamatergic synaptic transmission, slices were pre-incubated in aCSF containing LRRK2-IN-1 (1 μM) for 1 h before being placed in the recording chamber where they were perfused with aCSF containing LRRK2-IN-1 (1 μM).

2.12 | Statistical analysis

The GraphPad Prism 8 software (RRID: SCR_002798) was used for data analysis and statistics. Data are expressed as mean ± SEM with n indicating the number of neurons or mice tested. We used the Kolmogorov–Smirnov test to assess normal distribution of the data. To confirm the statistical power of our sample size, we performed a post hoc power analysis based on our results that show an altered glutamate release probability. We used the ClinCalc.com website (https://clincalc.com/) for this analysis (WT vs. G2019S; 0.05 for probability of type I error), and we obtained the following result: 87.9% for the post hoc power, which indicates a good estimation of our sample size. No test for outliers has been applied and no data points were excluded. Statistical significance of the results was assessed by using the Student's unpaired *t*-test, Mann–Whitney U test, nested one-way ANOVA followed by multiple comparisons (Tukey), nested t-test, two-way ANOVA followed by multiple comparisons (Tukey). All tests were two-tailed. We did not use data normalization for non-normally distributed datasets. Significant levels were set at $P < 0.05$. The results of the statistical analyses and detailed statistics are presented in Table S1.

3 | RESULTS

3.1 | G2019S mice display hyperlocomotion and increased exploratory behavior

We examined motor and non-motor behaviors in 10–12 months old WT and G2019S mice with five different behavioral tests. In the open field test, the total distance covered was significantly higher ($p < 0.01$; Figure 1b), and the time spent in the periphery of the arena was lower ($p < 0.05$; Figure 1c), in G2019S mice compared with WT mice. G2019S mice also displayed increased number of rearings ($p < 0.01$; Figure 1d). Male G2019S mice displayed an increased total distance covered and female G2019S mice displayed a tendency for an increased number of rearings (Figure S1). G2019S mice seemed to show reduced anxiety-like behavior because they spent less time in the periphery of the arena, and thus more time in the center, compared with WT mice (Lipkind et al., 2004). To examine this possibility, we performed two additional tests, that is, the light/dark test and the EPM test. These tests did not reveal any significant differences between G2019S and WT mice (Figure 1f–i). We assessed fine motor coordination and balance with the beam walking test and the pole test, and we found that G2019S mice and WT mice performed comparably in these two tests (Figure 1j–m). There were no sex-related differences in the beam walking test and the pole test (Figure S1). These results show that G2019S mice do not display motor impairment or anxiety-like behavior, but they display hyperlocomotion and increased exploratory behavior.

3.2 | Integrity of SNc- and VTA-DA neurons

We investigated whether the integrity of SNc- and VTA-DA neurons was altered in 10–12 months old G2019S mice. Immunohistochemistry of tyrosine hydroxylase (TH), the rate-limiting enzyme in the synthesis of DA, labeled neurons in the VTA and in the SNc with no differences in the number of TH-positive neurons between G2019S and WT mice in these two brain regions (Figure 2a–c). We also assessed the integrity of DA innervation of the dorsal striatum (which receives DA inputs mostly from the SNc) and the nucleus accumbens (which receives DA inputs mostly from the VTA) by measuring, with

western blotting, the protein amounts of TH and of the DA transporter (DAT). We found that these amounts were similar in G2019S and WT mice (Figure 2d–g).

We then performed whole-cell patch-clamp recordings in brain slices to assess if the electrophysiological properties of DA neurons differed between G2019S and WT mice. Although the numbers of male and female mice used in some of these experiments are small and variable, we did not observe sex-related differences in the measured membrane and synaptic properties. The intrinsic membrane properties (Figure S2) and action potential characteristics (Figure S3) were similar in WT and G2019S mice. Cell-attached recordings of the spontaneous action potential firing showed that the firing frequency (Figure 2h,k) and the regularity of firing (assessed with the coefficient of variation of interspike intervals, Figure 2i,l) of SNc- and VTA-DA neurons were not different between WT mice, G2019S mice in aCSF and G2019S mice in presence of the LRRK2 kinase inhibitor LRRK2-IN-1 (1 μM). These results show that SNc- and VTA-DA neurons are tonically active in 10–12 months old G2019S and WT mice and that their neurophysiological properties are unchanged in G2019S mice compared with WT mice.

3.3 | Altered glutamatergic synaptic transmission in midbrain DA neurons in G2019S mice

We examined the properties of glutamatergic synaptic transmission in DA neurons in the SNc and in the VTA of WT and G2019S mice. Spontaneous AMPAR-mediated EPSCs (sEPSCs) were measured, during 3–5 min-long recordings, in neurons voltage-clamped at - 80 mV. We selected an amplitude threshold of 5 pA based on the distribution of noise and sEPSC amplitude (Figure S4). In SNc-DA neurons, sEPSC amplitude was similar in WT mice, G2019S mice in aCSF and G2019S mice in LRRK2-IN-1 (1 μM), however, sEPSC frequency was lower in G2019S compared with WT mice ($p < 0.05$; Figure 3a-c). In the presence of LRRK2-IN-1, the sEPSC frequency in G2019S mice was similar to that measured in WT mice ($p = 0.8714$; Figure 3b). We also measured AMPAR-mediated EPSCs evoked by electrical stimulation of the slice, and we analyzed the paired-pulse ratio of two successive AMPAR-EPSCs, a measure of presynaptic modulation of glutamate release. We observed a paired-pulse depression at all interstimulus intervals in both WT and G2019S mice. However, at a short interstimulus interval (20 ms), this depression was significantly smaller in G2019S mice compared with WT mice (Figure 3d, e). Paired-pulse depression was not observed in SNc-DA neurons from G2019S mice in the presence of LRRK2-IN-1 (1 μM). However, no synaptic depression was observed in WT mice in the presence of LRRK2-IN-1 either (Figure S5), suggesting that endogenous LRRK2 kinase activity in WT and G2019S mice modulates glutamatergic synaptic transmission in SNc-DA neurons. We measured EPSCs mediated by NMDARs, evoked by electrical stimulation of the slice, in neurons voltage-clamped at +40 mV. The ratio between AMPAR-EPSC and NMDAR-EPSC (AMPA/NMDA ratio), a measure of long-term synaptic plasticity (Thomas & Malenka, 2003), was unaltered in G2019S mice as compared with WT mice (Figure 3f, g). These results demonstrate that SNc-DA neurons of G2019S mice do not develop alterations in long-term plasticity at glutamatergic synapses. However, a decreased sEPSC frequency and a decreased paired-pulse depression demonstrate an altered initial release probability at glutamatergic synapses in SNc-DA neurons of G2019S mice, which could be a consequence of an increased LRRK2 kinase activity.

In VTA-DA neurons, the amplitude of sEPSCs was significantly larger in G2019S compared with WT mice ($p < 0.01$), but the frequency of sEPSCs was similar in WT and G2019S mice (Figure 4a–c). In the presence of LRRK2-IN-1 (1 μM), the sEPSC amplitude in VTA-DA neurons from G2019S mice was similar to that measured in WT mice ($p = 0.7802$; Figure 4a). The paired-pulse ratio of two successive AMPAR-EPSCs showed facilitation at a 20 ms interval and depression at 100 and 1000 ms. The paired-pulse ratio was similar in WT and G2019S mice at all intervals (Figure 4d,e). The AMPA/NMDA ratio was unaltered in G2019S mice (Figure 4f,g). These results show that, unlike in the SNc, glutamate release is not altered in VTA-DA neurons of G2019S mice. However, postsynaptic changes, such as a modified content of AMPARs, might contribute to the increased sEPSC amplitude in VTA-DA neurons of G2019S mice.

3.4 | Altered glutamatergic markers in the ventral midbrain of G2019S mice

We tested the possibility that altered glutamatergic synaptic transmission in DA neurons of G2019S mice is associated with a change in postsynaptic and presynaptic markers of glutamatergic synapses in the ventral midbrain. Although the numbers of male and female mice used in these experiments are variable, we did not observe sex-related differences in the results obtained. Using immunohistochemistry, we found that the GluA1 subunit of AMPARs and the GluN1 subunit of NMDARs are co-expressed with TH-positive neurons in the SNc and VTA of both WT and G2019S mice (Figure 5a,b). To quantify the protein amounts of these postsynaptic markers of glutamatergic synapses, we performed Western blotting experiments and we found that the protein amounts of GluA1 and GluN1 in the ventral midbrain were significantly lower in G2019S mice as compared with WT mice ($p < 0.05$, Figure 5c,d). We also examined the presence of the vesicular glutamate transporter 1 (VGLUT1), a marker of glutamatergic presynaptic terminals originating in the cortex and hippocampus (Fremeau et al. 2004). The protein amounts of VGLUT1 were lower in the ventral midbrain of G2019S mice compared with WT mice ($p < 0.05$, Figure 5e).

4 | DISCUSSION

In the present study, we describe alterations in glutamatergic synaptic transmission in midbrain-DA neurons of middle-aged G2019S mice, before their degeneration and before the occurrence of motor

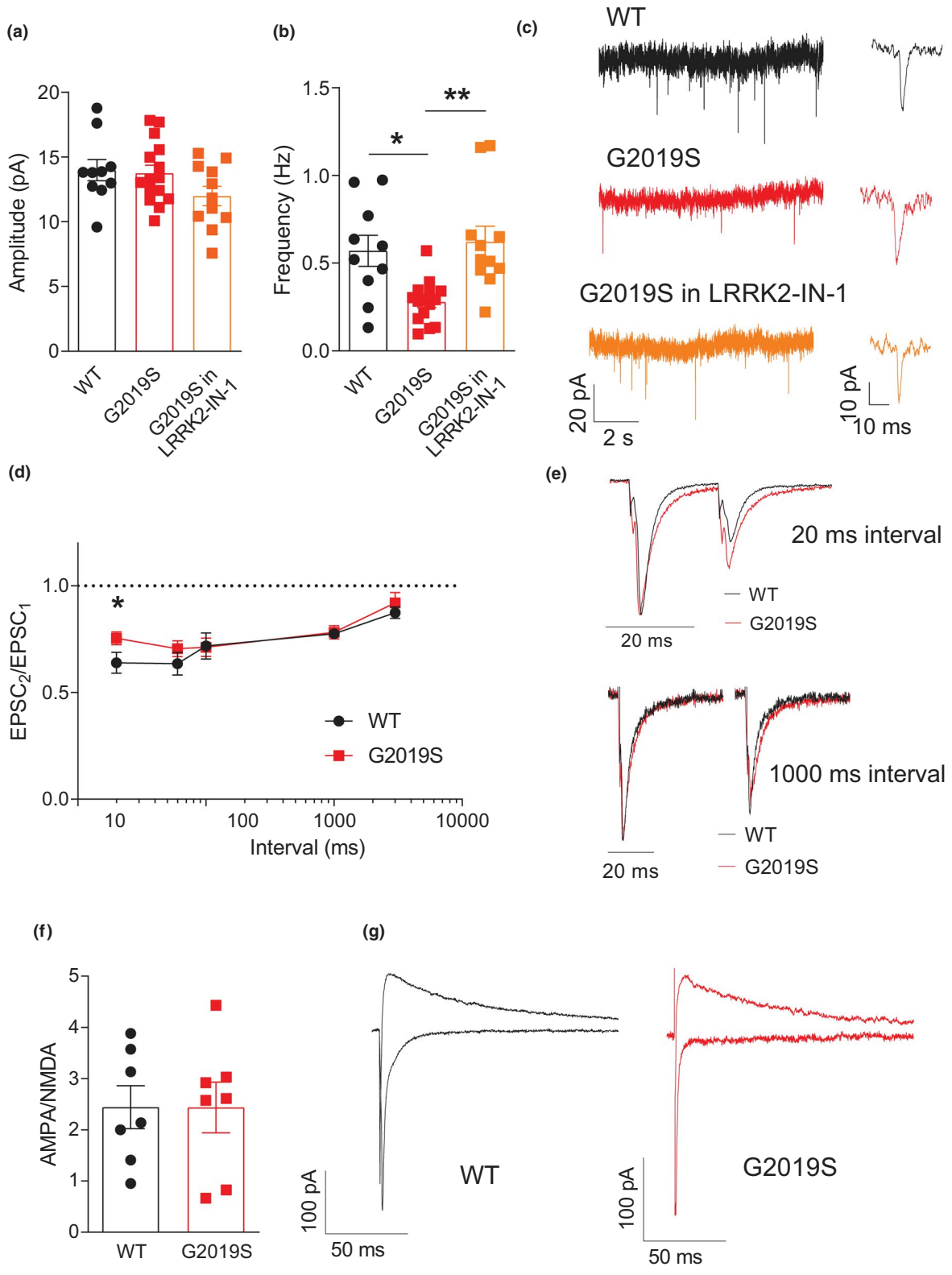

FIGURE 3 Glutamatergic synaptic transmission in SNc-DA neurons. Amplitude (a) and frequency (b) of sEPSCs measured in SNc-DA neurons ($n = 10$ cells from 4 WT mice, $n = 15$ cells from 7 G2019S mice in aCSF, and $n = 11$ cells from 4 G2019S mice in LRRK2-IN-1, 1 μM). * $p < 0.05$, ** $p < 0.01$ nested one-way ANOVA followed by multiple comparisons (Tukey). (c) Example recordings from three SNc-DA neurons in a WT mouse, a G2019S mouse in aCSF, and a G2019S mouse in LRRK2-IN-1. Traces on the right are examples of single sEPSCs. (d, e) paired-pulse ratio of two successive AMPAR-EPSCs at various interstimulus intervals ($n = 10$ cells from six WT mice and $n = 16$ cells from nine G2019S mice). * $p < 0.05$ nested t-test. Traces in (e) are examples of recordings of paired EPSCs in WT and G2019S mice evoked at 20 ms and 1000 ms intervals. (f, g) Ratio between AMPAR-EPSCs and NMDAR-EPSCs in SNc-DA neurons ($n = 7$ cells from 3 WT mice and $n = 7$ cells from 6 G2019S mice). Traces in (g) are examples of recordings of AMPAR-EPSCs (recorded at −80 mV) and NMDAR-EPSCs (recorded at +40 mV)

deficits, typical of Parkinsonism. We have shown that glutamate release onto SNc-DA neurons is decreased, and that presynaptic and postsynaptic markers of glutamatergic transmission are altered in the ventral midbrain of G2019S mice. We found that the changes seen in G2019S mice, compared to WT mice, are rescued in the presence of LRRK2-IN-1, suggesting that these changes are linked to an increased LRRK2 kinase activity. Our findings suggest that presynaptic and postsynaptic mechanisms in glutamatergic synapses might contribute to dysfunctions of DA neurons in the prodromal phase of Parkinsonism.

To investigate the roles of LRRK2 and mutated LRRK2 in the development of Parkinsonism, several rodent models have been generated with different methods, including bacterial artificial chromosomes (BACs) and knock-in (KI), to express human or murine LRRK2 or LRRK2-G2019S (Kuhlmann & Milnerwood, 2020; Pischedda & Piccoli, 2021). In accordance with previous studies demonstrating mild phenotypes in LRRK2-G2019S mice (Kuhlmann & Milnerwood, 2020; Volta & Melrose, 2017), we found that 10–12 months old G2019S mice did not display anxiety-like behaviors, and that their fine motor coordination and balance were unaltered, compared with age-matched WT littermates. G2019S mice, however, displayed an increased locomotion and rearing, demonstrating an increased exploratory behavior. These behaviors were described in other BAC and KI LRRK2-G2019S mice of the same age range or younger than the mice used in the present study (Longo et al., 2014; Volta et al., 2015; Volta et al., 2017; Yue et al., 2015). It was further demonstrated that enhanced LRRK2 kinase activity was responsible for hyperlocomotion in G2019S mice. Indeed, BAC mice overexpressing wild-type LRRK2 and KI mice carrying a kinase-dead mutation did not display increased locomotion and exploratory behavior. In addition, administration of a LRRK2 kinase inhibitor to G2019S mice reversed hyperkinesia, demonstrating that this behavior likely arises because of an increased LRRK2 kinase activity caused by the G2019S mutation (Longo et al., 2014). Further demonstration of hyperlocomotion in a different PD model, that is, young, but not old, mice overexpressing α-synuclein, suggests that hyperkinesia might be associated with an early increase in DA content in the striatum, which precedes neurodegeneration in aging mice (Mann & Chesselet, 2015). Taken together, these observations from different PD models, demonstrate that the BAC LRRK2-hG2019S model used in the present study is well suited to decipher cellular dysfunctions in DA neurons which occur before the onset of PD-like motor and non-motor impairments.

We found that the integrity of DA neurons was preserved in 10–12 months old G2019S mice, with intact protein amounts of TH and DAT in the striatum and in the nucleus accumbens, and no loss of TH-positive neurons in the SNc or in the VTA, suggesting a lack of DA deficits and absence of degeneration. These results are in accordance with previous studies from G2019S mice that are less than 1 year old, but contrast with the reported increased DAT level and function in the striatum of 12-months old G2019S KI mice (Kuhlmann & Milnerwood, 2020; Longo et al., 2017). In old (around 15–20 months) G2019S mice, however, mitochondrial abnormalities, altered DA release, reduced striatal DA innervation were observed in conjunction with motor impairments (Li et al., 2010; Lim et al., 2018; Melrose et al., 2010; Volta & Melrose, 2017; Yue et al., 2015). In addition to an intact striatal DA innervation and unchanged number of SNc- and VTA-DA neurons, we found that the intrinsic membrane properties of DA neurons were unaltered in G2019S mice compared with WT mice. This indicates that intrinsic ion channel functions underlying membrane properties are intact in these neurons. Furthermore, the pacemaker firing in SNc- and VTA-DA neurons was similar in G2019S mice compared with WT mice.

The present study identifies postsynaptic and presynaptic alterations in glutamatergic synapses onto midbrain DA neurons of G2019S mice. We found a reduced protein amount of the GluA1 and GluN1 subunits of AMPARs and NMDARs, respectively, in the ventral midbrain, which was, however, not associated with a change in the AMPA/NMDA ratio in SNc- and VTA-DA neurons. This could indicate a decrease in both AMPARs and NMDARs at glutamatergic synapses, but the amplitude of sEPSCs was not altered in SNc-DA neurons and it was increased in VTA-DA neurons. Different mechanisms could account for a change in sEPSC amplitude in VTA-DA neurons. One of these mechanisms could involve the change in the subunit composition of AMPARs, in particular, the contribution of the GluA2 subunit. The changes in the protein amounts might not reflect receptors at the membrane of DA neurons that contribute to synaptic transmission but might indicate a reduced intracellular pool of receptors in DA neurons, as well as in non-DA neurons. Indeed, unpublished data from our group indicate that GABAergic neurons in the substantia nigra reticulata do not display changes in synaptic AMPARs and NMDARs. A region-specific alteration in presynaptic regulation of glutamatergic synaptic transmission is the most striking change that we found in G2019S mice. In SNc-DA neurons of WT mice, glutamatergic synapses displayed paired-pulse depression which indicates a high initial release probability and is likely accounted for by a decrease in release probability and a decrease in quantal content during the second stimulus (Chen et al., 2004; Debanne et al., 1996). In SNc-DA neurons of G2019S mice, paired-pulse depression was decreased and sEPSC frequency was also decreased, demonstrating a reduced initial release probability. The amplitude of sEPSC was increased in VTA-DA neurons which was not accompanied by a change in sEPSC frequency or in the paired-pulse ratio, demonstrating a lack of presynaptic alteration of glutamate release. Intact presynaptic glutamatergic function was also observed in the hippocampus of 8–12 months old G2019S mice (Sweet et al., 2015), further supporting the region-specificity in the presynaptic changes induced by the G2019S mutation. An altered release probability in SNc-DA neurons of G2019S mice indicates that the molecular machinery responsible for exocytosis of glutamate is modified, likely through an increased LRRK2 kinase activity in glutamatergic axon terminals. Our results with the LRRK2 kinase inhibitor support this hypothesis although the absence of paired-pulse depression in the presence of LRRK2-IN-1 in WT and G2019S mice remains to be further investigated. LRRK2 plays key roles in presynaptic control of neurotransmitter release by regulating synaptic

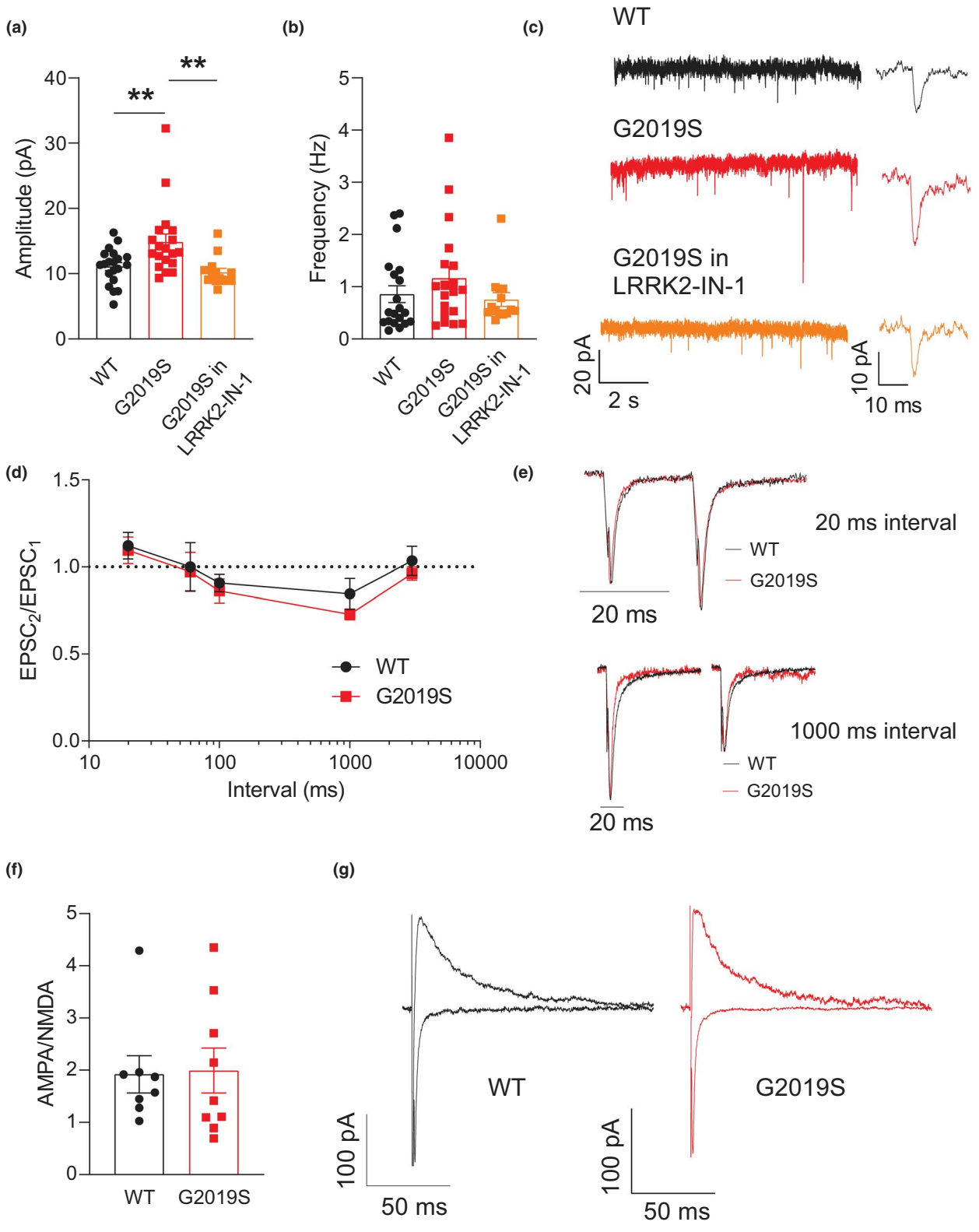

FIGURE 4 Glutamatergic synaptic transmission in VTA-DA neurons. Amplitude (a) and frequency (b) of sEPSCs measured in VTA-DA neurons ($n = 20$ cells from eight WT mice, $n = 19$ cells from seven G2019S mice in aCSF, and $n = 14$ cells from thre G2019S mice in LRRK2-IN-1). ** $p < 0.01$ nested one-way ANOVA followed by multiple comparisons (Tukey). (c) Example recordings from three VTA-DA neurons in a WT mouse, a G2019S mouse in aCSF, and a G2019S mouse in LRRK2-IN-1. Traces on the right are examples of single sEPSCs. (d, e) paired-pulse ratio of two successive AMPAR-EPSCs at various interstimulus intervals ($n = 9$–13 cells from four WT mice and $n = 8$–10 cells from eight G2019S mice). Traces in (e) are examples of recordings of paired EPSCs in WT and G2019S mice evoked at 20 ms and 1000 ms intervals. (f, g) Ratio between AMPAR-EPSCs and NMDAR-EPSCs in VTA-DA neurons ($n = 8$ cells from five WT mice and $n = 9$ cells from seven G2019S mice). Traces in (g) are examples of recordings of AMPAR-EPSCs (recorded at −80 mV) and NMDAR-EPSCs (recorded at +40 mV)

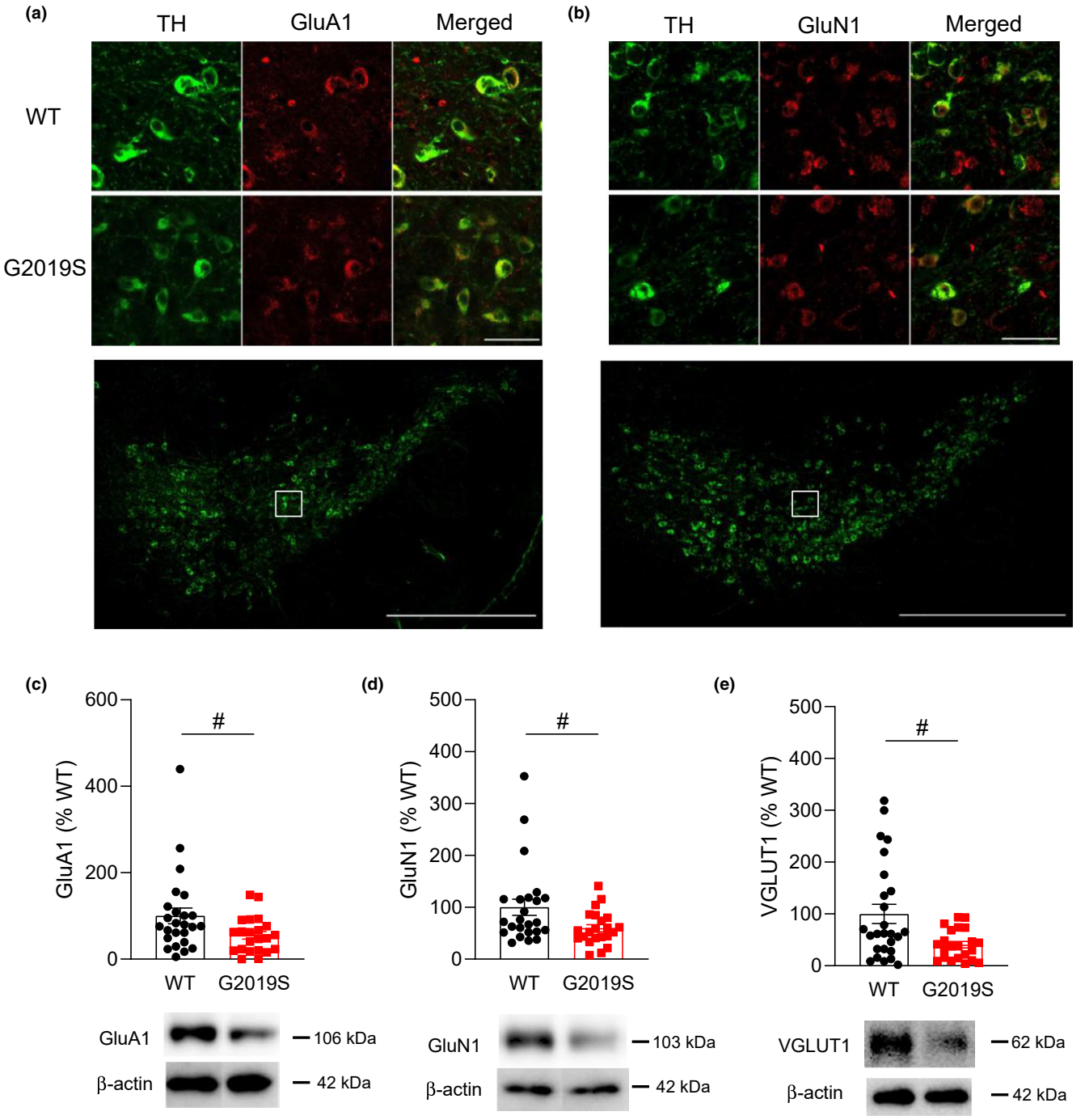

FIGURE 5 Altered protein amounts of markers of glutamatergic synapses in the ventral midbrain. (a, b) Upper panel: Immunofluorescence detection of TH (green), GluA1 (a, red) and GluN1 (b, red) in the medial SNc of a WT mouse and a G2019S mouse. TH-positive neurons were co-labeled with GluA1 (a) and GluN1 (b) (scale bars 50 μm, 18 z-stacks with 2 μm interval). Lower panel: Lower magnification image indicating, with the white square, the location of the higher magnification upper panels in the medial SNc (Scale bar 500 μm). (c–e) Western blotting of GluA1 (c), GluN1 (d), and VGLUT1 (e) in the ventral midbrain of WT mice ($n = 24–25$) and G2019S mice ($n = 22$). # $p < 0.05$ Mann–Whitney test

vesicle recycling/endocytosis, and the G2019S mutation was shown to decrease synaptic vesicle endocytosis (Belluzzi et al., 2012; Pan et al., 2017; Pischedda & Piccoli, 2021). Altered phosphorylation of LRRK2 substrates, such as Rab GTPases (Pfeffer, 2018; Steger et al., 2016), in glutamatergic presynaptic terminals in the SNc might contribute to dysregulated glutamate release and possibly also to the degeneration of axons arising from the cortex in LRRK2-G2019S mice (Jeong et al., 2018). Other glutamatergic projections to midbrain DA neurons may also be affected by the G2019S mutation, in particular those arising in nuclei involved in motor control and shown to be dysfunctional in PD, that is, the subthalamic nucleus and pedunculopontine tegmental nucleus.

Our study suggests a potential mechanism by which LRRK2-G2019S could modulate glutamate release in the SNc, that is, by interfering with the function of VGLUT1 and thereby reducing vesicular glutamate content. Indeed, we found that VGLUT1 is reduced in the ventral midbrain, which could underlie the decreased paired-pulse depression in SNc-DA neurons of G2019S mice. Interestingly, in PD patients, there is a reduced VGLUT1 expression in cortical regions known to provide glutamatergic inputs to SNc and VTA neurons (Kashani et al., 2007). How a reduced glutamate release probability and an altered vesicular glutamate content could contribute to degeneration of SNc-DA neurons is beyond the scope of the present study and remains to be examined. Nonetheless, a change in the balance of excitatory inputs onto SNc-DA neurons, and not onto VTA-DA neurons, may be a prodromal sign of DA neuron dysfunction.

In conclusion, our study describes region-specific alterations in glutamatergic synapses onto midbrain DA neurons in a mouse model of familial late-onset PD. Our findings pave the way for future studies aiming to decipher the potential role of altered glutamatergic synapses onto SNc-DA neurons in behavioral and neurochemical modifications linked to the G2019S-LRRK2 mutation. Because there are similarities between familial PD linked to LRRK2 mutation and sporadic PD, our findings shed insights into the mechanisms that might contribute to the pathophysiology of idiopathic and familial PD.

ACKNOWLEDGMENTS

We thank Dr. Xiaoqun Zhang for valuable advice and help with the mouse genotyping. This work was supported by the Swedish Research Council (Vetenskapsrådet, grant 2018–02979), Parkinsonfonden, Parkinson Research Foundation (Sweden), Åhlén-Stiftelsen, Karolinska Institutet funding for Ph.D. student, Karolinska Institutet research fund, Loo and Hans Osterman Foundation for Medical Research, Gun & Bertil Stohnes Stiftelse and Stiftelsen för ålderssjukdomar vid Karolinska Institutet. These funding bodies had no role in the study design; in the collection, analysis, and interpretation of data; in the writing of the report; and in the decision to submit the article for publication. The flowchart in Figure 1a was created with BioRender (https://biorender.com/).

All experiments were conducted in compliance with the ARRIVE guidelines.

CONFLICT OF INTEREST

The authors declare no conflict of interest.

AUTHOR CONTRIBUTIONS

Olga Skiteva: Formal analysis, Investigation, Writing - Original Draft, Writing - Review & Editing, Visualization. Ning Yao: Formal analysis, Investigation, Writing - Review & Editing, Visualization. Giacomo Sitzia: Investigation, Writing - Original Draft, Writing - Review & Editing, Visualization. Karima Chergui: Conceptualization, Resources, Writing - Original Draft, Writing - Review & Editing, Supervision, Project administration, Funding acquisition.

DATA AVAILABILITY STATEMENT

The data that support the findings of this study are available from the corresponding author upon reasonable request.

ORCID

Giacomo Sitzia https://orcid.org/0000-0003-2244-4393
Karima Chergui https://orcid.org/0000-0001-5702-0422

REFERENCES

Beccano-Kelly, D. A., Kuhlmann, N., Tatarnikov, I., Volta, M., Munsie, L. N., Chou, P., Cao, L. P., Han, H., Tapia, L., Farrer, M. J., & Milnerwood, A. J. (2014). Synaptic function is modulated by LRRK2 and glutamate release is increased in cortical neurons of G2019S LRRK2 knock-in mice. *Frontiers in Cellular Neuroscience*, 8, 301.

Belluzzi, E., Gonnelli, A., Cirnaru, M. D., Marte, A., Plotegher, N., Russo, I., Civiero, L., Cogo, S., Carrion, M. P., Franchin, C., Arrigoni, G., Beltramini, M., Bubacco, L., Onofri, F., Piccoli, G., & Greggio, E. (2016). LRRK2 phosphorylates pre-synaptic N-ethylmaleimide sensitive fusion (NSF) protein enhancing its ATPase activity and SNARE complex disassembling rate. *Molecular Neurodegeneration*, 11, 1.

Belluzzi, E., Greggio, E., & Piccoli, G. (2012). Presynaptic dysfunction in Parkinson's disease: A focus on LRRK2. *Biochemical Society Transactions*, 40, 1111–1116.

Brichta, L., & Greengard, P. (2014). Molecular determinants of selective dopaminergic vulnerability in Parkinson's disease: An update. *Frontiers in Neuroanatomy*, 8, 152.

Chen, C., Soto, G., Dumrongprechachan, V., Bannon, N., Kang, S., Kozorovitskiy, Y., & Parisiadou, L. (2020). Pathway-specific dysregulation of striatal excitatory synapses by LRRK2 mutations. *eLife*, 9, 1–26.

Chen, G., Harata, N. C., & Tsien, R. W. (2004). Paired-pulse depression of unitary quantal amplitude at single hippocampal synapses. *Proceedings of the National Academy of Sciences of the United States of America*, 101, 1063–1068.

Chou, J. S., Chen, C. Y., Chen, Y. L., Weng, Y. H., Yeh, T. H., Lu, C. S., Chang, Y. M., & Wang, H. L. (2014). (G2019S) LRRK2 causes early-phase dysfunction of SNpc dopaminergic neurons and impairment of corticostriatal long-term depression in the PD transgenic mouse. *Neurobiology of Disease*, 68, 190–199.

Cresto, N., Gaillard, M.-C., Gardier, C., Gubinelli, F., Diguet, E., Bellet, D., Legroux, L., Mitja, J., Auregan, G., Guillermier, M., Josephine, C., Jan, C., Dufour, N., Joliot, A., Hantraye, P., Bonvento, G., Déglon, N., Bemelmans, A. P., Cambon, K., … Brouillet, E. (2020). The C-terminal domain of LRRK2 with the G2019S mutation is sufficient to produce neurodegeneration of dopaminergic neurons in vivo. *Neurobiology of Disease*, 134, 104614.

Debanne, D., Guerineau, N. C., Gahwiler, B. H., & Thompson, S. M. (1996). Paired-pulse facilitation and depression at unitary synapses in rat hippocampus: Quantal fluctuation affects subsequent release. *The Journal of Physiology*, 491(Pt 1), 163–176.

Di Maio, R., Hoffman, E. K., Rocha, E. M., Keeney, M. T., Sanders, L. H., De Miranda, B. R., Zharikov, A., Van Laar, A., Stepan, A. F., Lanz, T. A., Kofler, J. K., Burton, E. A., Alessi, D. R., Hastings, T. G., & Greenamyre, J. T. (2018). LRRK2 activation in idiopathic Parkinson's disease. *Science Translational medicine*, 10, eaar5429.

Feng, Z. J., Zhang, X., & Chergui, K. (2014). Allosteric modulation of NMDA receptors alters neurotransmission in the striatum of a mouse model of Parkinson's disease. *Experimental Neurology*, 255, 154–160.

Fremeau, R. T., Jr., Voglmaier, S., Seal, R. P., & Edwards, R. H. (2004). VGLUTs define subsets of excitatory neurons and suggest novel roles for glutamate. *Trends in Neurosciences*, 27, 98–103.

Gcwensa, N. Z., Russell, D. L., Cowell, R. M., & Volpicelli-Daley, L. A. (2021). Molecular mechanisms underlying synaptic and axon degeneration in Parkinson's disease. *Frontiers in Cellular Neuroscience*, 15, 626128.

Giesert, F., Hofmann, A., Bürger, A., Zerle, J., Kloos, K., Hafen, U., Ernst, L., Zhang, J., Vogt-Weisenhorn, D. M., & Wurst, W. (2013). Expression analysis of Lrrk1, Lrrk2 and Lrrk2 splice variants in mice. *PLoS One*, 8, e63778.

Gould, T. D. (2009). *Mood and anxiety related phenotypes in mice characterization using behavioral tests: Neuromethods*. Humana Press.

Healy, D. G., Falchi, M., O'Sullivan, S. S., Bonifati, V., Durr, A., Bressman, S., Brice, A., Aasly, J., Zabetian, C. P., Goldwurm, S., Ferreira, J. J., Tolosa, E., Kay, D. M., Klein, C., Williams, D. R., Marras, C., Lang, A. E., Wszolek, Z. K., Berciano, J., … International LRRK2 Consortium. (2008). Phenotype, genotype, and worldwide genetic penetrance of LRRK2-associated Parkinson's disease: A case-control study. *The Lancet. Neurology*, 7, 583–590.

Henderson, M. X., Sedor, S., McGeary, I., Cornblath, E. J., Peng, C., Riddle, D. M., Li, H. L., Zhang, B., Brown, H. J., Olufemi, M. F., Bassett, D. S., Trojanowski, J. Q., & Lee, V. M. Y. (2020). Glucocerebrosidase activity modulates neuronal susceptibility to pathological α-synuclein insult. *Neuron*, 105, 822–836.e827.

Hernandez, D. G., Reed, X., & Singleton, A. B. (2016). Genetics in Parkinson disease: Mendelian versus non-mendelian inheritance. *Journal of Neurochemistry*, 139(Suppl 1), 59–74.

Higashi, S., Moore, D. J., Colebrooke, R. E., Biskup, S., Dawson, V. L., Arai, H., Dawson, T. M., & Emson, P. C. (2007). Expression and localization of Parkinson's disease-associated leucine-rich repeat kinase 2 in the mouse brain. *Journal of Neurochemistry*, 100, 368–381.

Jeong, G. R., Jang, E. H., Bae, J. R., Jun, S., Kang, H. C., Park, C. H., Shin, J. H., Yamamoto, Y., Tanaka-Yamamoto, K., Dawson, V. L., Dawson, T. M., Hur, E. M., & Lee, B. D. (2018). Dysregulated phosphorylation of Rab GTPases by LRRK2 induces neurodegeneration. *Molecular Neurodegeneration*, 13, 8.

Kashani, A., Betancur, C., Giros, B., Hirsch, E., & El Mestikawy, S. (2007). Altered expression of vesicular glutamate transporters VGLUT1 and VGLUT2 in Parkinson disease. *Neurobiology of Aging*, 28, 568–578.

Kuhlmann, N., & Milnerwood, A. J. (2020). A critical LRRK at the synapse? The neurobiological function and pathophysiological dysfunction of LRRK2. *Frontiers in Molecular Neuroscience*, 13, 153.

Li, X., Patel, J. C., Wang, J., Avshalumov, M. V., Nicholson, C., Buxbaum, J. D., Elder, G. A., Rice, M. E., & Yue, Z. (2010). Enhanced striatal dopamine transmission and motor performance with LRRK2 overexpression in mice is eliminated by familial Parkinson's disease mutation G2019S. *The Journal of Neuroscience: The Official Journal of The Society for Neuroscience*, 30, 1788–1797.

Lim, J., Bang, Y., Choi, J. H., Han, A., Kwon, M. S., Liu, K. H., & Choi, H. J. (2018). LRRK2 G2019S induces anxiety/depression-like behavior before the onset of motor dysfunction with 5-HT1A receptor upregulation in mice. *The Journal of Neuroscience: The Official Journal of The Society for Neuroscience*, 38, 1611–1621.

Lim, S. Y., & Lang, A. E. (2010). The nonmotor symptoms of Parkinson's disease-an overview. *Movement disorders: official journal of the Movement Disorder Society*, 25(Suppl 1), S123–S130.

Lipkind, D., Sakov, A., Kafkafi, N., Elmer, G. I., Benjamini, Y., & Golani, I. (2004). New replicable anxiety-related measures of wall vs. center behavior of mice in the open field. *Journal of Applied Physiology*, 97, 347–359.

Longo, F., Mercatelli, D., Novello, S., Arcuri, L., Brugnoli, A., Vincenzi, F., Russo, I., Berti, G., Mabrouk, O. S., Kennedy, R. T., Shimshek, D. R., Varani, K., Bubacco, L., Greggio, E., & Morari, M. (2017). Age-dependent dopamine transporter dysfunction and Serine129 phospho-alpha-synuclein overload in G2019S LRRK2 mice. *Acta Neuropathologica Communications*, 5, 22.

Longo, F., Russo, I., Shimshek, D. R., Greggio, E., & Morari, M. (2014). Genetic and pharmacological evidence that G2019S LRRK2 confers a hyperkinetic phenotype, resistant to motor decline associated with aging. *Neurobiology of Disease*, 71, 62–73.

Mann, A., & Chesselet, M.-F. (2015). Techniques for motor assessment in rodents. In M. S. LeDoux (Ed.), *Movement Disorders* (pp. 139–157). Academic Press.

Marte, A., Russo, I., Rebosio, C., Valente, P., Belluzzi, E., Pischedda, F., Montani, C., Lavarello, C., Petretto, A., Fedele, E., Baldelli, P., Benfenati, F., Piccoli, G., Greggio, E., & Onofri, F. (2019). Leucine-rich repeat kinase 2 phosphorylation on synapsin I regulates glutamate release at pre-synaptic sites. *Journal of Neurochemistry*, 150, 264–281.

Matikainen-Ankney, B. A., Kezunovic, N., Mesias, R. E., Tian, Y., Williams, F. M., Huntley, G. W., & Benson, D. L. (2016). Altered development of synapse structure and function in striatum caused by Parkinson's disease-linked LRRK2-G2019S mutation. *The Journal of Neuroscience: The Official Journal of The Society for Neuroscience*, 36, 7128–7141.

Melrose, H., Lincoln, S., Tyndall, G., Dickson, D., & Farrer, M. (2006). Anatomical localization of leucine-rich repeat kinase 2 in mouse brain. *Neuroscience*, 139, 791–794.

Melrose, H. L., Dachsel, J. C., Behrouz, B., Lincoln, S. J., Yue, M., Hinkle, K. M., Kent, C., Korvatska, E., Taylor, J. P., Witten, L., Liang, Y.-Q., Beevers, J. E., Boules, M., Serna, V., Gaukhman, A., Yu, X., Castanedes-Casey, M., Braithwaite, A. T., Ogholikhan, S., … Farrer, M. J. (2010). Impaired dopaminergic neurotransmission and microtubule-associated protein tau alterations in human LRRK2 transgenic mice. *Neurobiology of Disease*, 40, 503–517.

Moore, C., Xu, M., Bohlen, J. K., & Meshul, C. K. (2021). Differential ultrastructural alterations in the Vglut2 glutamatergic input to the substantia nigra pars compacta/pars reticulata following nigrostriatal dopamine loss in a progressive mouse model of Parkinson's disease. *The European Journal of Neuroscience*, 53, 2061–2077.

Pan, P. Y., Li, X., Wang, J., Powell, J., Wang, Q., Zhang, Y., Chen, Z., Wicinski, B., Hof, P., Ryan, T. A., & Yue, Z. (2017). Parkinson's disease-associated LRRK2 hyperactive kinase mutant disrupts synaptic vesicle trafficking in ventral midbrain neurons. *The Journal of Neuroscience: The Official Journal of The Society for Neuroscience*, 37, 11366–11376.

Pfeffer, S. R. (2018). LRRK2 and Rab GTPases. *Biochemical Society Transactions*, 46, 1707–1712.

Pischedda, F., Cirnaru, M. D., Ponzoni, L., Sandre, M., Biosa, A., Carrion, M. P., Marin, O., Morari, M., Pan, L., Greggio, E., Bandopadhyay, R., Sala, M., & Piccoli, G. (2021). LRRK2 G2019S kinase activity triggers neurotoxic NSF aggregation. *Brain*, 144, 1509–1525.

Pischedda, F., & Piccoli, G. (2021). LRRK2 at the pre-synaptic site: A 16-years perspective. *Journal of Neurochemistry*, 157, 297–311.

Qin, Q., Zhi, L. T., Li, X. T., Yue, Z. Y., Li, G. Z., & Zhang, H. (2017). Effects of LRRK2 inhibitors on nigrostriatal dopaminergic neurotransmission. *CNS Neuroscience & Therapeutics*, 23, 162–173.

Richard, I. H. (2005). Anxiety disorders in Parkinson's disease. *Advances in Neurology*, 96, 42–55.

Russo, S. J., & Nestler, E. J. (2013). The brain reward circuitry in mood disorders. *Nature Reviews. Neuroscience*, 14, 609–625.

Schindelin, J., Arganda-Carreras, I., Frise, E., Kaynig, V., Longair, M., Pietzsch, T., Preibisch, S., Rueden, C., Saalfeld, S., Schmid, B., Tinevez, J. Y., White, D. J., Hartenstein, V., Eliceiri, K., Tomancak, P., & Cardona, A. (2012). Fiji: An open-source platform for biological-image analysis. *Nature Methods*, 9, 676–682.

Sitzia, G., Mantas, I., Zhang, X., Svenningsson, P., & Chergui, K. (2020). NMDA receptors are altered in the substantia nigra pars reticulata and their blockade ameliorates motor deficits in experimental parkinsonism. *Neuropharmacology*, 174, 108136.

Spatola, M., & Wider, C. (2014). Genetics of Parkinson's disease: The yield. *Parkinsonism & Related Disorders*, 20(Suppl 1), S35–S38.

Steger, M., Tonelli, F., Ito, G., Davies, P., Trost, M., Vetter, M., Wachter, S., Lorentzen, E., Duddy, G., Wilson, S., Baptista, M. A. S., Fiske, B.

K., Fell, M. J., Morrow, J. A., Reith, A. D., Alessi, D. R., & Mann, M. (2016). Phosphoproteomics reveals that Parkinson's disease kinase LRRK2 regulates a subset of Rab GTPases. *eLife*, 5, e12813.

Sveinbjornsdottir, S. (2016). The clinical symptoms of Parkinson's disease. *Journal of Neurochemistry*, 139(Suppl 1), 318–324.

Sweet, E. S., Saunier-Rebori, B., Yue, Z., & Blitzer, R. D. (2015). The Parkinson's disease-associated mutation LRRK2-G2019S impairs synaptic plasticity in mouse hippocampus. *The Journal of Neuroscience: The Official Journal of The Society for Neuroscience*, 35, 11190–11195.

Thomas, M. J., & Malenka, R. C. (2003). Synaptic plasticity in the mesolimbic dopamine system. *Philosophical Transactions of the Royal Society of London. Series B, Biological Sciences*, 358, 815–819.

Tozzi, A., Durante, V., Bastioli, G., Mazzocchetti, P., Novello, S., Mechelli, A., Morari, M., Costa, C., Mancini, A., di Filippo, M., & Calabresi, P. (2018). Dopamine D2 receptor activation potently inhibits striatal glutamatergic transmission in a G2019S LRRK2 genetic model of Parkinson's disease. *Neurobiology of Disease*, 118, 1–8.

Vitte, J., Traver, S., Maues De Paula, A., Lesage, S., Rovelli, G., Corti, O., Duyckaerts, C., & Brice, A. (2010). Leucine-rich repeat kinase 2 is associated with the endoplasmic reticulum in dopaminergic neurons and accumulates in the core of Lewy bodies in Parkinson disease. *Journal of Neuropathology and Experimental Neurology*, 69, 959–972.

Volta, M., Beccano-Kelly, D. A., Paschall, S. A., et al. (2017). Initial elevations in glutamate and dopamine neurotransmission decline with age, as does exploratory behavior, in LRRK2 G2019S knock-in mice. *eLife*, 6, e28377.

Volta, M., Cataldi, S., Beccano-Kelly, D., Munsie, L., Tatarnikov, I., Chou, P., Bergeron, S., Mitchell, E., Lim, R., Khinda, J., Lloret, A., Bennett, C. F., Paradiso, C., Morari, M., Farrer, M. J., & Milnerwood, A. J. (2015). Chronic and acute LRRK2 silencing has no long-term behavioral effects, whereas wild-type and mutant LRRK2 overexpression induce motor and cognitive deficits and altered regulation of dopamine release. *Parkinsonism & Related Disorders*, 21, 1156–1163.

Volta, M., & Melrose, H. (2017). LRRK2 mouse models: Dissecting the behavior, striatal neurochemistry and neurophysiology of PD pathogenesis. *Biochemical Society Transactions*, 45, 113–122.

Wang, J., Wang, F., Mai, D., & Qu, S. (2020). Molecular mechanisms of glutamate toxicity in Parkinson's disease. *Frontiers in Neuroscience*, 14, 585584.

West, A. B., Cowell, R. M., Daher, J. P., Moehle, M. S., Hinkle, K. M., Melrose, H. L., Standaert, D. G., & Volpicelli-Daley, L. A. (2014). Differential LRRK2 expression in the cortex, striatum, and substantia nigra in transgenic and nontransgenic rodents. *The Journal of Comparative Neurology*, 522, 2465–2480.

Xiong, Y., Neifert, S., Karuppagounder, S. S., Liu, Q., Stankowski, J. N., Lee, B. D., Ko, H. S., Lee, Y., Grima, J. C., Mao, X., Jiang, H., Kang, S. U., Swing, D. A., Iacovitti, L., Tessarollo, L., Dawson, T. M., & Dawson, V. L. (2018). Robust kinase- and age-dependent dopaminergic and norepinephrine neurodegeneration in LRRK2 G2019S transgenic mice. *Proceedings of the National Academy of Sciences of the United States of America*, 115, 1635–1640.

Yao, N., Skiteva, O., Zhang, X., Svenningsson, P., & Chergui, K. (2018). Ketamine and its metabolite (2R,6R)-hydroxynorketamine induce lasting alterations in glutamatergic synaptic plasticity in the mesolimbic circuit. *Molecular Psychiatry*, 23, 2066–2077.

Yue, M., Hinkle, K. M., Davies, P., Trushina, E., Fiesel, F. C., Christenson, T. A., Schroeder, A. S., Zhang, L., Bowles, E., Behrouz, B., Lincoln, S. J., Beevers, J. E., Milnerwood, A. J., Kurti, A., McLean, P. J., Fryer, J. D., Springer, W., Dickson, D. W., Farrer, M. J., & Melrose, H. L. (2015). Progressive dopaminergic alterations and mitochondrial abnormalities in LRRK2 G2019S knock-in mice. *Neurobiology of Disease*, 78, 172–195.

SUPPORTING INFORMATION

Additional supporting information may be found in the online version of the article at the publisher's website.

How to cite this article: Skiteva, OP, Yao, N, Sitzia, G, Chergui, K (2022) LRRK2-G2019S mice display alterations in glutamatergic synaptic transmission in midbrain dopamine neurons. *Journal of Neurochemistry*. 161:158–172. https://doi.org/10.1111/jnc.15588